Modification of the coordination environment of Eu2+ in Sr2SiO4:Eu2+ phosphors to achieve full color emission

Journal:	*Journal of Materials Chemistry C*
Manuscript ID:	TC-ART-07-2014-001435.R1
Article Type:	Paper
Date Submitted by the Author:	17-Oct-2014
Complete List of Authors:	Ju, Li-Cheng; University of Science and Technology of China, Department of Materials Science and Engineering Xu, Xin; University of Science and Technology of China, Department of Materials Science and Engineering Hao, Lu-Yuan; University of Science and Technology of China, Department of Materials Science and Engineering Lin, Yue; University of Science and Technology of China, Lee, Ming-Hsien; Department of Physics,

Journal Name

Dynamic Article Links▶

ARTICLE TYPE

Modification of the coordination environment of Eu^{2+} in Sr_2SiO_4:Eu^{2+} phosphors to achieve full color emission

Li-Cheng Ju,[a] Xin Xu,*[a] Lu-Yuan Hao,[a] Yue Lin,[b] and Ming-Hsien Lee[c]

5 The Sr_2SiO_4:Eu^{2+} phosphors were synthesized by a conventional solid state reaction method. After a low amount of nitrogen (~1 mol% of oxygen) was incorporated to modify the local coordination environment of Eu^{2+}, the phosphor showed a single intense broad band emission centered at 625 nm under the blue light (453 nm) excitation, and three bands (480, 555 and 625nm) emission under ultraviolet radiation. The incorporation of nitrogen could be confirmed by the X-ray photoelectron spectroscopy (XPS), Fourier-
10 Transform Infrared spectroscopy (FT-IR) and absorption spectra. The 480 and 555 nm emissions originate from Eu^{2+} ions occupying the Sr(I) sites and Sr(II) sites in Sr_2SiO_4 crystal, respectively, while the 625 nm emission originates from the nitrogen coordinated Eu^{2+} ions. The local coordination structure around Eu^{2+} ions in the red phosphors was analyzed with the aid of density functional theory based first principles calculations. The analysis showed that nitrogen should preferentially substitute the O5' sites
15 around Eu^{2+} in Sr(II) sites, which agreed fairly well with the experimental results from the X-ray absorption fine structure (XAFS) and the electron paramagnetic resonance (EPR) spectra. The electronic structure analysis confirmed the lowered center of gravity of Eu 5d energy states and the broadened Eu 4f energy states, which is due to the tightened coordination environment and the hybridization of 4f states of Eu and 2p states of nitrogen/oxygen, leading to the red emission. The novel nitrogen modified
20 Sr_2SiO_4:Eu^{2+} could serve as a full color phosphor for near-UV LEDs or a red-emitting phosphor for blue LEDs.

1 Introduction

The InGaN-based white-light-emitting diodes (WLEDs) lighting has drawn great attention, due to its advantages in energy
25 efficiency, long lifetime, compactness, environment friendly and designable features. As an indispensable constituent part in WLEDs, the phosphors make big contributions to the color index and efficiency.

Among the various phosphors, red phosphors play a key role in
30 improving the color rendering property of WLEDs and are the most urgent to be improved. Traditional powerful red emitting phosphors (i.e. Y_2O_3:Eu^{3+}) cannot be used in WLEDs due to their line excitation and emission.[1] The sulfide phosphors (i.e. $Sr_{1-x}Ca_xS$:Eu^{2+}) with stronger emission intensity under the blue
35 light excitation suffer from low stability against humid, thermal and radiative environments.[2] Recently, the oxynitride phosphors, such as $CaAlSiN_3$:Eu^{2+},[3-5] $M_2Si_5N_8$:Eu^{2+} (M = Ca, Sr, Ba),[6-12] were found to be very promising red phosphors. However, they require severe synthesis conditions, such as elevated pressure and
40 temperature, air-sensitive starting powders.[10, 13, 14] To overcome these problems, it is essential to develop novel red phosphors that can be easily prepared and emit bright red light under the excitation of near UV-blue lights.

As a kind of traditional phosphor, Eu^{2+} doped strontium
45 orthosilicate (Sr_2SiO_4) phosphors have attracted intense interests due to their special structural features and potential applications in developing WLEDs.[15-17] Sr_2SiO_4 has two crystallographic phases: monoclinic (β-Sr_2SiO_4) and orthorhombic (α'-Sr_2SiO_4). The two phases can coexist, as the phase transformation occurs
50 through a short-range rearrangement of the coordination structure without breaking any bonds.[18-20] There are two cation sites of Sr^{2+} in both β-Sr_2SiO_4 and α'-Sr_2SiO_4 phases: Sr(I) is ten-coordinated and Sr(II) is nine-coordinated by oxygen atoms within a limited range.[21] When Eu occupies Sr(I) site with weak crystal filed, the
55 emission band is about 470-490nm, while the Sr(II) site has a more compact environment and stronger crystal field effect, leading to a longer emission wavelength of 540-570nm.[20] Bond lengths in Sr polyhedra are scattered over a wider range of values in the β-Sr_2SiO_4 phase than in the α'-Sr_2SiO_4 phases,[22] leading to
60 a slight blue-shift of Eu^{2+} in the β-Sr_2SiO_4 phase for both Sr(I) and Sr(II) sites. Through structural modification, the Sr_2SiO_4:Eu^{2+} phosphors could be controlled to emit different colors in a wide range, from blue to yellow.[23]

Recently, red-emitting Sr_2SiO_4:Eu^{2+} phosphors have been
65 reported through the incorporation of nitrogen.[24-26] $Sr_2SiN_2O_{4-1.5z}$:Eu^{2+} (0.7 < z < 1.2) reported by Wang $et\ al.$ had a stoichiometric composition,[26] and the red emission was attributed to the overlapped two bands due to the Eu(I) and Eu(II) sites, while $Sr_2Si(O_{1-x}N_x)_4$:Eu^{2+} reported by Kim $et\ al.$ was considered
70 as a non-stoichiometric solid-solution with the substitution of N^{3-} for O^{2-},[24, 25] and the red emission was assigned to the Eu(II) sites. Both of them focused on the photoluminescence properties and simply ascribed the red emission to the strong crystal field splitting and the nephelauxetic effect of N^{3-}. However, no
75 detailed study has been done on the coordination environment of

Eu^{2+}, and the interaction mechanism of nitrogen on red-shift emission.

Unlike the references[24-26], where a large amount of nitrogen was incorporated, we succeeded in achieving a strong red-emission in the $Sr_2SiO_4:Eu^{2+}$ phosphors through the incorporation of a very low amount of nitrogen in this paper. The preferential nitrogen substitution sites in the host lattice, the local structural deformation after nitrogen doping and the relationship between photoluminescence and the coordination environment of Eu^{2+} were determined with the aid of geometry optimization and electronic structure calculations, performed with the Cambridge Serial Total Energy Package (CASTEP) code. This code employs density functional theory (DFT), pseudopotential, and a plane-wave basis set to provide a good atomic-level description of all manners of materials and molecules.[27-30]

2 Experimental Section

2.1 Synthesis

Nitrogen modified $Sr_2SiO_4:Eu^{2+}$ phosphors (denoted as NSSO) were prepared by a traditional solid-state reaction method. A mixture of $1.97SrCO_3$-$0.97SiO_2$-$0.01Si_3N_4$-$0.015Eu_2O_3$, as the raw materials, was calcined at 1500 ^oC for 4 h in BN crucibles by a tube furnace under flowing NH_3 atmosphere. Both the heating and cooling rates were 300^oC/h. For comparison, $Sr_2SiO_4:Eu^{2+}$ phosphors (denoted as SSO) were synthesized by firing a mixture of $1.97SrCO_3$-SiO_2-$0.015Eu_2O_3$ under the same preparation procedure. The produced samples were benignly crushed into fine powders. We use $Sr_2Si_5N_8:Eu^{2+}$ phosphor as the reference of red light emission, which is prepared by solid-state reaction method in our laboratory.

2.2 Characterization

The crystalline phases developed in the final products were identified by X-ray diffraction analysis (XRD, Philips PW 1700; Cu $K_{\alpha1}$ radiation; scanning rate of 2 ^{o}/min) adding KCl as the internal standard. The ratio of α'-Sr_2SiO_4 phase to β-Sr_2SiO_4 phase is calculated based on the intensity of distinguishable peaks around 27.5^o.

The photoluminescence (PL) spectra under UV–vis excitation were measured using a fluorescent spectrophotometer (F-4600, Hitachi Ltd., Japan) with a 200 W Xe lamp as the excitation source. High temperature luminescence measurements were carried out on the same spectrophotometer equipped with a heating element. The absorption spectra were recorded with a UV-vis-NIR spectrophotometer equipped with an integrating sphere (SolidSpec-3700, Shimadzu, Tokyo, Japan).

The quantum efficiency (QE) were conducted with a 200 W Xe lamp as an excitation source and a Hamamatsu MPCD-7000 multichannel photodetector. The decay curves were measured by a steady state/transient fluorescence spectrometer (JY Fluorolog-3-Tou, JobinYvon, France).

The morphology of the synthesized phosphors was measured by a scanning electron microscope (SEM, JED-2300, JEOL, Japan). High resolution transmission electron microscope (HRTEM) image and the diffraction pattern were obtained from a spherical aberration corrected JEM-ARM 200F.

X-ray photoelectron spectroscopy (XPS) measurements were performed on an ESCALAB 250 high performance electron spectrometer using a monochromatized Al Kα excitation source. Fourier-Transform Infrared spectra (FT-IR) were measured on a Nicolet 8700 spectrophotometer in the range 400-4000 cm^{-1} using the KBr pellet (~1 wt%) method. Each analysis consisted of a minimum 32 scans and the resolution was 4 cm^{-1}.

The X-ray absorption spectra at Eu L_3-edge were measured on the beam line BL14W1 of Shanghai Synchrotron Radiation Facility (SSRF) in Shanghai, China. The electron beam energy was 3.5 GeV and the mean stored current was 300 mA.

Room temperature Electron Paramagnetic Resonance (EPR) spectra were obtained using a JEOL JES-FA200 EPR spectrometer (300 K, 9.057 GHz, X-band). Microwave power employed was 1mW; sweep width ranged from 2800 to 3700 G. Modulation frequency and modulation amplitude were 100 kHz and 3.5 G, respectively.

2.3 First principles calculation

We calculated the crystal structures' optimization and electronic structures of the SSO and NSSO phosphors by first principles' method. Based on the experimental data, we use Eu doped α'-Sr_2SiO_4 (SSO) as the control group. We build a $1\times2\times1$ supercell of α'-Sr_2SiO_4 and replace one Sr with Eu in the cell as the SSO model. Then, we substitute each oxygen coordinating Eu by nitrogen to establish one NSSO model. These models were optimized using the Cambridge Sequential Total Energy Package (CASTEP) computational codes. These calculations employ density functional theory plane-wave pseudopotential method. PBE method by Generalized Gradient-corrected Approximation (GGA) was used for the exchange correlation potential. The optimized lattice structures are used for calculating the electronic structures and density of states of these phosphors. The basic parameters for both parts were chosen as follows: The kinetic energy cutoff is 430 eV, sets of k points are $4\times2\times3$, self-consistent field tolerance thresholds are 1.0×10^{-6} eV/atom and the space representation is reciprocal. The reliability of the calculation was demonstrated by the result of the convergence test. We use a 1.9 eV scissors operator to plot the band structure of SSO in order to compare with NSSO.

3 Results and Discussion

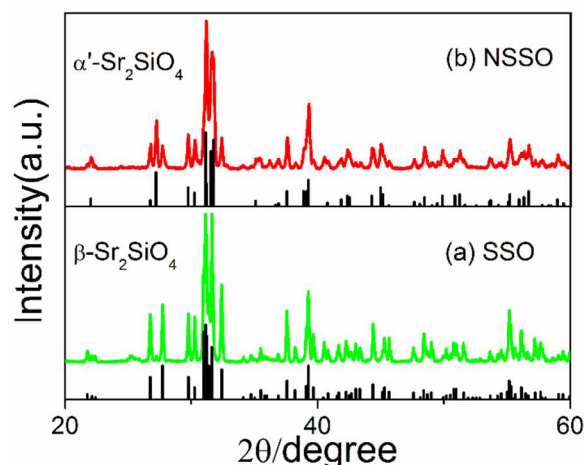### 3.1 Phases and photoluminescence properties

Fig. 1 The XRD patterns of (a) SSO and (b) NSSO.

Fig.1 shows the XRD patterns of the SSO and NSSO phosphors. All the diffraction peaks could be attributed to Sr_2SiO_4 phases. SSO only shows monoclinic (β-Sr_2SiO_4) phase, which is in good agreement with that reported before.[20] While NSSO exhibits mainly orthorhombic phase (α'-Sr_2SiO_4) with about 30% β-Sr_2SiO_4.
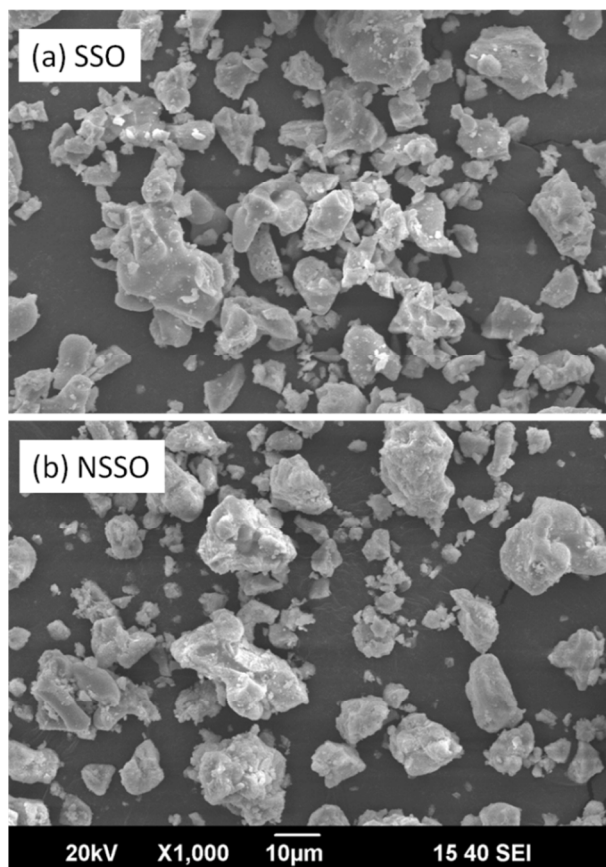

Fig. 2 SEM image of the SSO and NSSO phosphors.

Fig.2 shows an electron microscope image of the SSO and NSSO phosphors. The mostly equiaxed shaped crystals of 5-10 μm size could be seen for both phosphors. The nitrogen incorporation exhibits little influence on the morphology and particle size of the phosphors.

Fig.3 shows the photoluminescence properties of SSO, NSSO and $Sr_2Si_5N_8$:Eu^{2+} phosphors. SSO exhibits two emission bands centered at 470 nm from Eu ions in Sr (I) sites and 540 nm from Eu ions in Sr (II) sites, which in good agreement with that reported previously[20, 31]. However, NSSO phosphor shows an extra emission peak at 625 nm besides the two traditional peaks at 480 nm and 555 nm. As reported previously[20], pure α'-Sr_2SiO_4:Eu^{2+} phosphor exhibits two emission bands centered at 490/570 nm. Because NSSO contains a small amount of β phase, we could conclude that the 480 nm emissions of the NSSO phosphors are from Eu ions in Sr(I) sites of α' and β phase, and the 555 nm emissions are from Eu ions in Sr(II) sites of α' and β phase, as reported before.[20] In addition, the emission band centered at 625 nm are very similar to the emission spectra of $Sr_2Si_5N_8$:Eu^{2+} phosphor.[13] Considering the similar shapes of their excitation spectra, we can infer that some of the Eu^{2+} ions in the NSSO phosphor are coordinated with nitrogen.

Photoluminescence properties indicate that the NSSO phosphors could serve as a full color phosphor for near-UV LEDs or a red-emitting phosphor for blue LEDs. Fig.4 shows the SSO and NSSO phosphors under 365 nm excitation and under natural light. The SSO phosphor looks quite different from the NSSO phosphor, which is in good agreement with their photoluminescence properties.
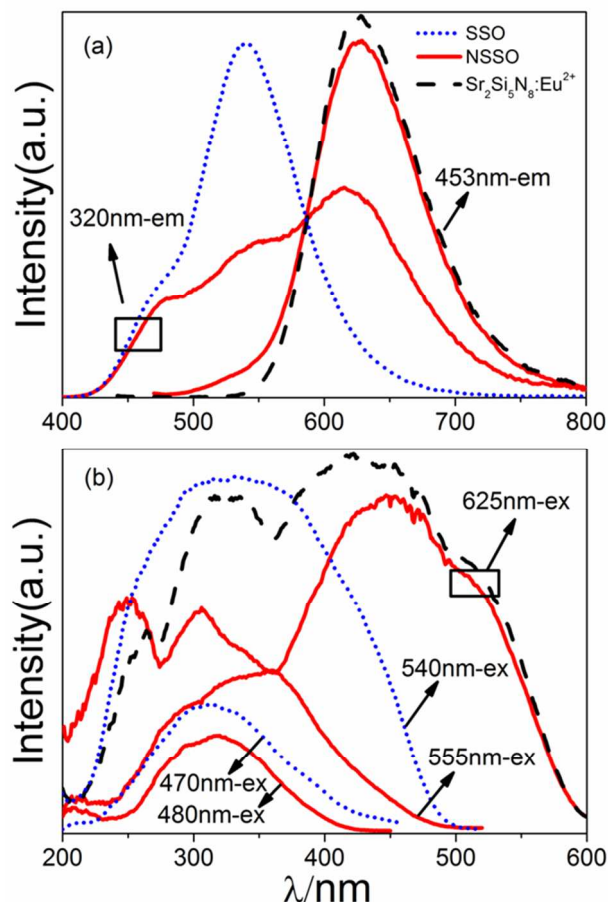

Fig. 3 The (a) emission and (b) excitation spectra of SSO ($\cdots$), NSSO (—) and $Sr_2Si_5N_8$:Eu^{2+} phosphor ($---$).
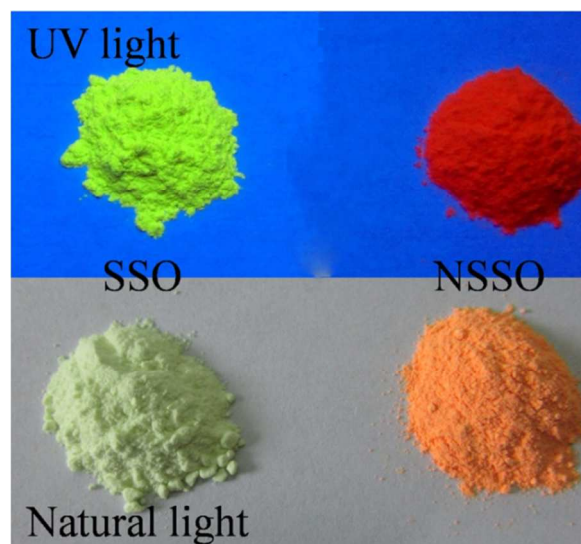

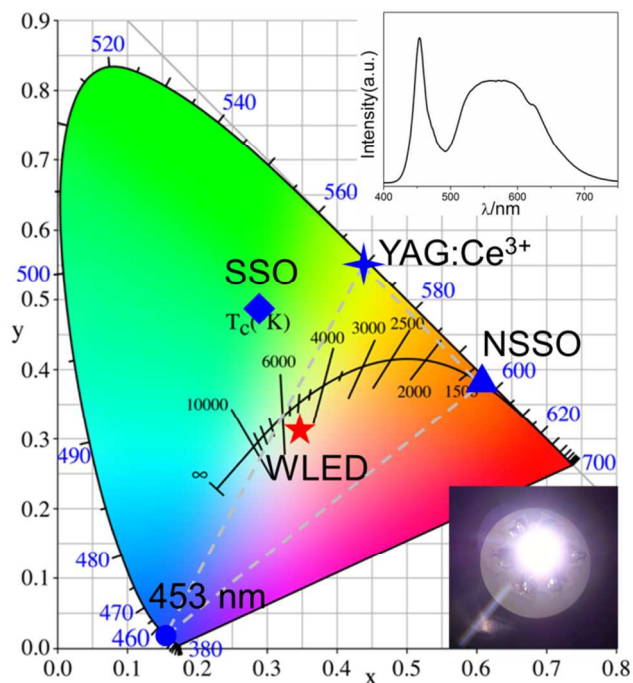**Fig. 4** Images of SSO and NSSO under UV and natural light.

Fig. 5 The CIE color coordinates of SSO (excited by 320 nm), NSSO (excited by 453 nm), commercial YAG:Ce³⁺ (excited by 453 nm) and a white-emitting GaN-based LED packaged by NSSO and commercial
5 YAG:Ce³⁺ phosphor (insets: emission spectra of the wLED [upper right] and the real image of it [lower right]).

The decay for the 625 nm emission of NSSO under 453 nm excitation could be fitted using one exponential function with a decay time of 1037 ns, which is similar to 1360 ns of
10 $Sr_2Si_5N_8:Eu^{2+}$. [32] The external QE of the red emission of NSSO at the excitation wavelength of 453 nm reaches 68.4%, which are expected to be increased through removing the small particles shown in Fig.2.

Fig.5 plots the corresponding Commission Internationale de
15 l'Eclairage (CIE) 1931 chromaticity coordinates. The CIE color coordinates of NSSO indicates its high color saturation, so it could compensate for the red color deficiency of the current cold YAG:Ce³⁺-based WLEDs[33]. A white-emitting LED lamp presenting a warm color temperature of 4814 K has been realized
20 using the NSSO phosphor in combination with the commercial YAG:Ce³⁺ phosphor, as shown in the lower right inset of Fig.5. The CIE chromaticity coordinates (*0.345, 0.307*) for the fabricated LED lamp lie in the white light region. The emission spectrum of the LED lamp is also shown in the upper right inset
25 of Fig.5, which exhibits good color rendering index of 91 for R_a. The CIE chromaticity coordinates (*x, y*) and the correlated color temperature (CCT) for the fabricated LEDs can be tuned by changing the addition amount of NSSO.
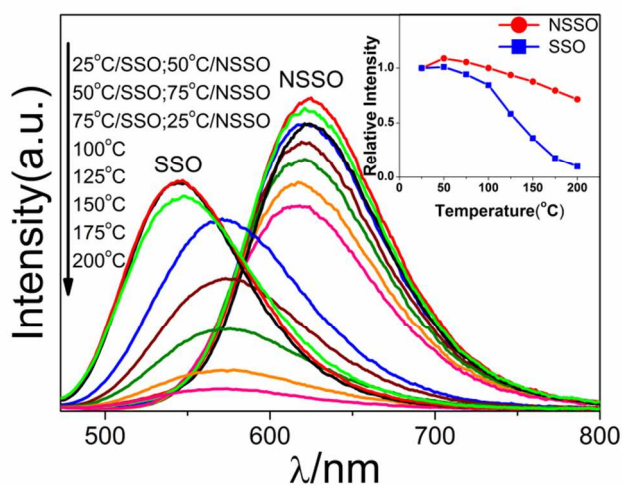

30 **Fig. 6** Temperature dependence of emission spectra of SSO and NSSO excited at 453 nm. The inset shows the variation of PL intensity as a function of temperature.

The thermal stability of phosphors plays a key role in the high power WLEDs. Fig.6 shows the temperature dependence of the
35 PL properties for the SSO and NSSO phosphors under the excitation at 453 nm. The inset shows the variation of PL intensity as a function of temperature. SSO exhibits a steady loss of emission intensity with the increase of temperature and remains only about 36.0% of the initial intensity, when the
40 measuring temperature is up to 150 °C. While for NSSO, PL intensity increases with the temperature first.[34] With the increase in the temperature up to 150 °C, NSSO only shows a decrease of 12.3%. It should be pointed out that the pure α' $Sr_2SiO_4:Eu^{2+}$ phosphor[20] exhibits similar thermal quenching properties
45 (remains about 41% at 150 °C) as SSO, indicating that the thermal stability of NSSO could not be attributed to the α' phase. High temperature will increase the probability of non-radiative transition, which is caused by thermal activation and release of the luminescent center through the crossing point between the
50 excited state and the ground state. The activation energy of non-radiative transition increases with the increase of the crystal stiffness and the decrease of the Eu^{2+} mobility. The nitrogen coordination will suppress the Eu^{2+} vibration, which could also be confirmed by the smaller stokes shift (~6000 cm⁻¹) of NSSO,
55 compared with that (~10000 cm⁻¹) of SSO.

The blue-shift of NSSO with increasing temperature could be explained by the thermally active phonon-assisted tunnelling from the excited states of lower-energy emission band to those of higher-energy emission band in the configuration coordinate
60 diagram.[24, 28] The red-shift of SSO with increasing temperature could be attributed to the Varshni equation,[35] which points out that the increase of temperature reduces the transition energy between excited and ground states. While, the sudden red-shift of the emission wavelength in SSO is due to the phase
65 transformation from β- to α'-Sr_2SiO_4 at 85 °C, because the phase transformation occurs through a short-range rearrangement of the coordination structure without breaking any bonds.[21, 36]

As reported before, a complex phosphor consisting of 64 wt% $Sr_2Si_5N_8:Eu^{2+}$ and 36 wt% $Sr_2SiO_4:Eu^{2+}$ was obtained through the
70 chemical reaction of $SrCO_3$, Eu_2O_3, and Si_3N_4.[37] However, that phosphor strangely exhibited equivalent optical properties with

pure $Sr_2Si_5N_8:Eu^{2+}$ phosphors. Based on our research, the $Sr_2SiO_4:Eu^{2+}$ obtained there actually is the nitrogen modified $Sr_2SiO_4:Eu^{2+}$, which has comparable photoluminescence with $Sr_2Si_5N_8:Eu^{2+}$ phosphors.

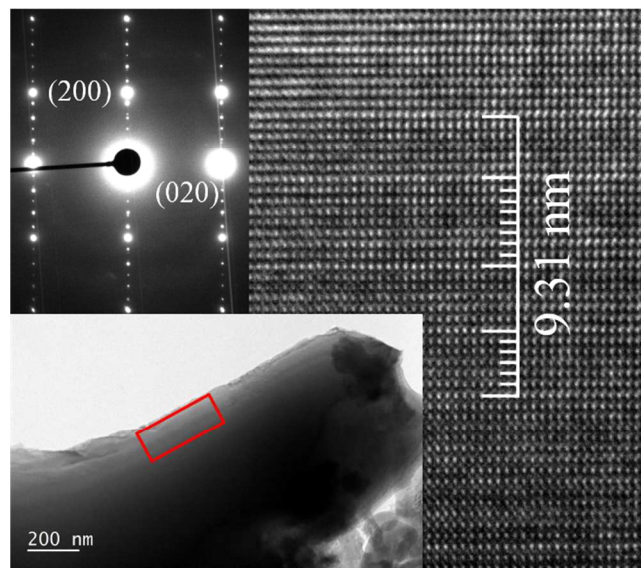**3.2 Experimental Results Related to Structural and Photoluminescence Features**

Fig. 7 Selected area electron diffraction pattern and corresponding lattice image of NSSO phosphor. Incident beam is almost parallel to the orthorhombic c-axis.
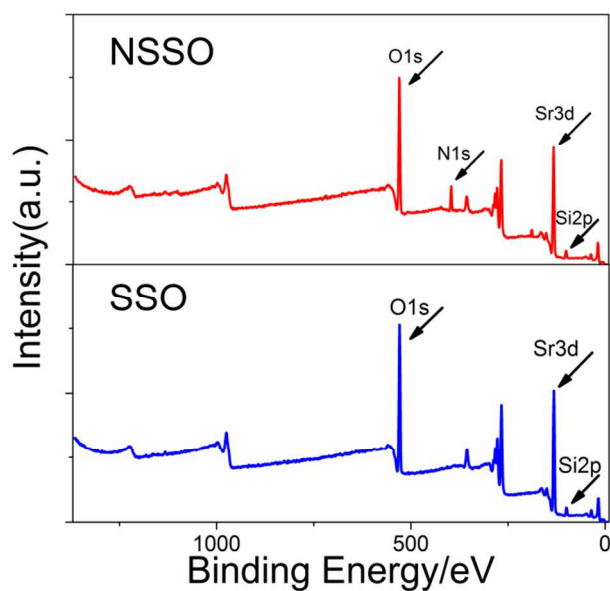

Fig. 8 XPS spectra of SSO and NSSO phosphors.

Fig.7 shows the selected area electron diffraction (SAED) pattern and corresponding lattice image of NSSO phosphor. The SAED pattern of NSSO phosphor is successfully indexed with the orthorhombic α'-Sr_2SiO_4 cell and clearly shows the existence of long periodicity. The corresponding lattice image confirms that the crystal is characterized by a superlattice structure. However, the periodicity is not regular throughout the whole lattice area, as shown in Fig.7. Some long periodicities include six interplanar

spacings of (200), which is a systematic absence crystal plane in normal lattice and appears under the effects of the modulated structure. Meanwhile, eight interplanar spacings' long periodicity also presents in our lattice image. The formation of superlattice is due to the ordered doping of impurity atoms. Based on our experimental data, SSO phosphor does not show a superlattice structure. (not shown here) Therefore, we exclude the possibility of Eu ions' ordered doping and conclude that it is the orderly doped nitrogen leading to the superlattice structure of NSSO. Then a little bit non-regular long periodicity indicates that nitrogen impurity does not show a perfectly ordered distribution in the base material. From Fig.7, we can calculate that the average long periodicity is about 2.325 nm, which are about six and a half interplanar spacings of (200).

Fig.8 shows the XPS spectra of SSO and NSSO. NSSO has nitrogen impurity appeared in their surfaces, which provides chemical foundations for the formation of microstructures similar to nitride. In contrast, SSO phosphor doesn't show peaks of N 1s electrons.
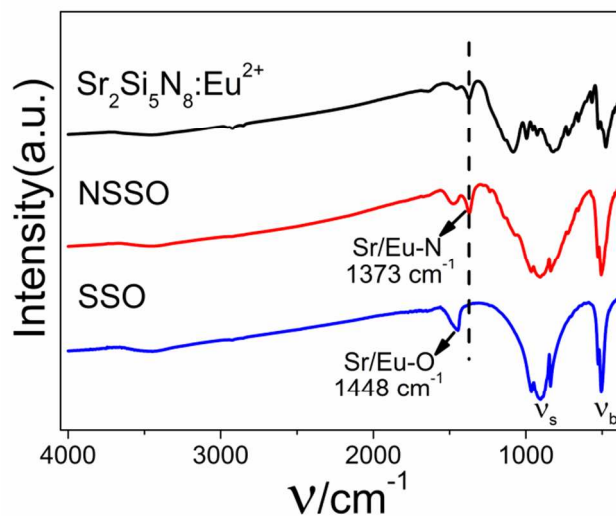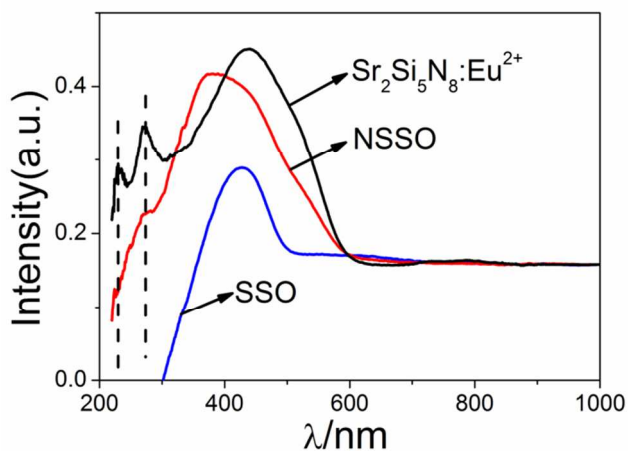

Fig. 9 FT-IR spectra of SSO, NSSO and $Sr_2Si_5N_8:Eu^{2+}$ phosphors.

Fig. 10 Absorption spectra of the SSO, NSSO and $Sr_2Si_5N_8:Eu^{2+}$ phosphors.

Fig.9 exhibits the FT-IR spectra of the SSO, NSSO and $Sr_2Si_5N_8:Eu^{2+}$ phosphors. The peak of Sr/Eu-N bond vibration

appears in NSSO, while the SSO sample doesn't show such peaks.[38] Absorption spectra relate to the PL properties since most of the absorbed energy can turn into the excitation energy. Fig.10 shows the absorption spectra of the SSO, NSSO and $Sr_2Si_5N_8:Eu^{2+}$ phosphors. The absorption spectrum of NSSO at shorter wavelength is similar to that of the $Sr_2Si_5N_8:Eu^{2+}$ phosphor. It seems that the absorption spectrum of NSSO is a combination of SSO and $Sr_2Si_5N_8:Eu^{2+}$ phosphors. Fig.9 and Fig.10 confirm that nitrogen does enter the crystal structure and forms chemical bonds with surrounding Sr/Eu ions in the NSSO phosphor.

Based on the above experimental results and their XRD patterns in Fig.1, we conclude that $Sr_2SiO_4:Eu^{2+}$ phosphor can tolerate a local structural modification around Eu^{2+} ions through nitrogen incorporation. This might be partly attributed to the chemical similarity of oxygen and nitrogen, and another important reason is the slack lattice structure and loosely coordinated metal ions in the Sr_2SiO_4 crystal structure, in other word, components' high freedom of motion or rotation in the crystals. Actually, the nitrogen content in the $Sr_2SiO_4:Eu^{2+}$ phosphor could also be varied in a large range, but all of them show similar photoluminescence properties, which is in good agreement with that reported before.[26] In our opinion, only nitrogen directly coordinated to Eu^{2+} could modify the photoluminescence properties. Too much nitrogen incorporation might enter the host crystal and has little influence on the photoluminescence properties.
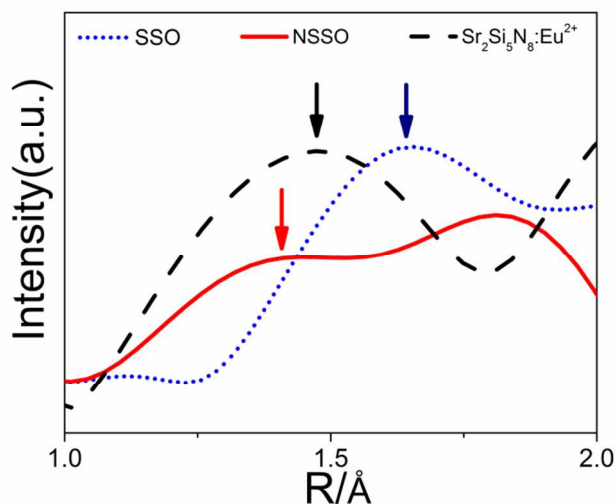

Fig. 11 Fourier transformed EXAFS spectra of SSO (···), NSSO (—) and $Sr_2Si_5N_8:Eu^{2+}$ phosphors (− − −).

In order to get direct information about the local coordination environment surrounding Eu ions, Fig.11 shows the Fourier transformed Eu L_3-edge Extended X-ray Absorption Fine Structure (EXAFS) spectra of the SSO, NSSO and $Sr_2Si_5N_8:Eu^{2+}$ phosphors.

A precise investigation of the O and N atoms coordinated with Eu^{2+} could not be achieved from EXAFS due to the complexity of crystal structure and the lack of model compound. However, a qualitative description could be given based on the EXAFS results. The average coordination distance of the first layer surrounding Eu ions in $Sr_2Si_5N_8:Eu^{2+}$ phosphor is much shorter than that in SSO phosphor, which could be ascribed to the short Eu-N bonding length. By comparing the EXAFS spectra of SSO and NSSO, we can clearly see that the first coordination shell around Eu^{2+} ions in NSSO has much shorter coordination distance.
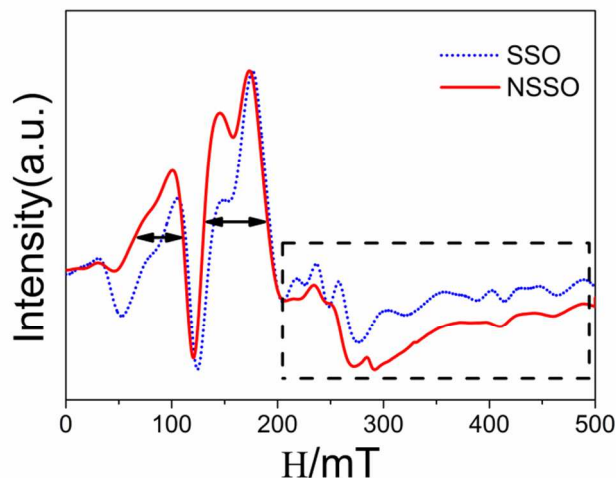

Fig. 12 EPR spectra of SSO and NSSO.

EPR is a powerful tool for studying the coordination environment of Eu^{2+} ions. Fig.12 gives the Electron Paramagnetic Resonance (EPR) results of SSO and NSSO. The resonant peaks are very complicated and hard to be treated theoretically due to two reasons: 1) the spin-orbital coupling effect for the unpaired electrons in 4f obitals; 2) Eu^{2+} ions are coordinated within the crystal field.[39] However, obvious difference can be observed in the results. The EPR peak width of NSSO is broader than that of SSO. We attribute it to the lifetime broadening which results from the spin-lattice interaction.[39] Based on the uncertainty principle, the stronger the interaction, the smaller the electrons' lifetime deviation, the bigger the bias of magnetic field intensity, therefore, the broader the peak width. So, it is clear that the unpaired electrons of Eu^{2+} ions in NSSO interact more intensively with the coordinated lattice and the crystal field around them is stronger.

Journal Name

ARTICLE TYPE
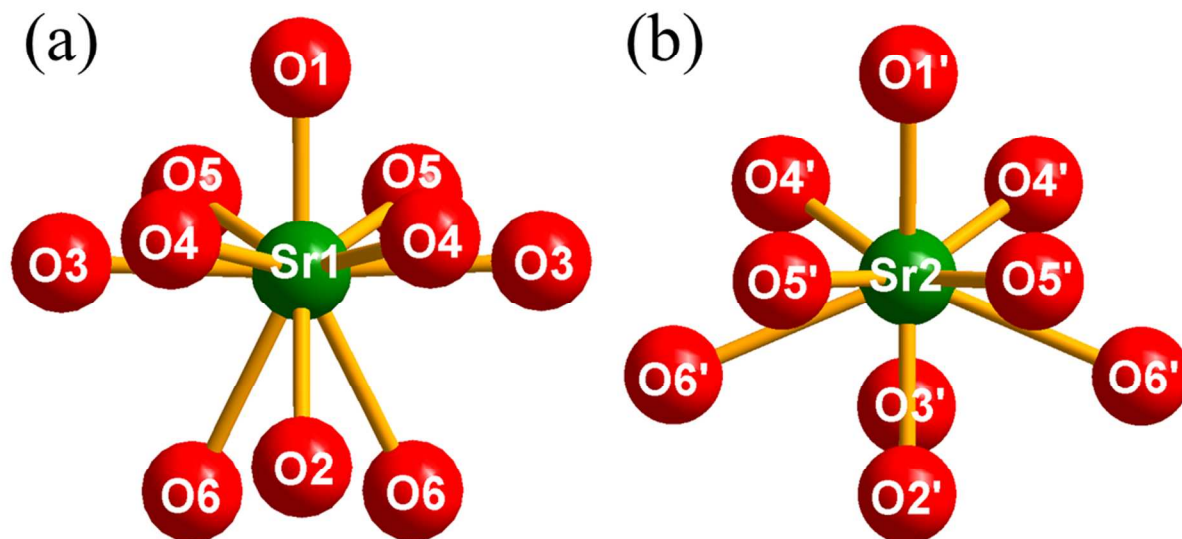
Fig. 13 Local structures of Sr sites in α'-Sr_2SiO_4.

3.3 First principles calculation

The experimental results in the previous sections show that the
5 incorporation of small amount of N in the lattice of Sr_2SiO_4:Eu^{2+}
leads to a new red emission. It is important to explore the
mechanism of the red emission through first-principles
calculations.[29, 30, 40]

As can be seen in Fig.13, there are six kinds of oxygen in either
10 Sr(I) or Sr(II) site according to their coordination distance and
crystal symmetry. Two SSO models could be built with one of
the two Sr sites occupied by Eu. Because of the low amount of
nitrogen incorporation, it is reasonable to assume that only one
oxygen is replaced by N in the supercell. So we substituted each
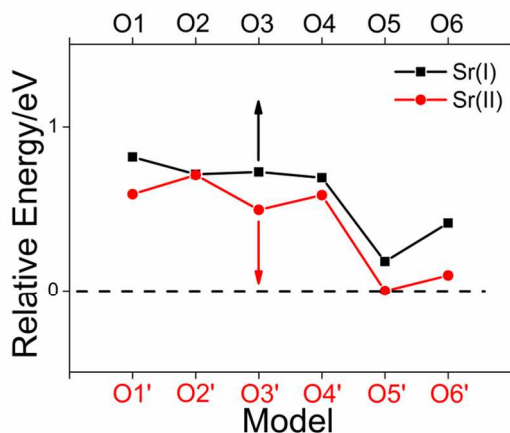15 kind of oxygen surrounding Eu by a nitrogen to establish the
NSSO models.

Fig. 14 Relative energy of NSSO models, Sr(I) and Sr (II) indicate the Eu
site, while O1-6 and O1'-6' indicate the N sites.

20 We first carried out full geometry relaxation for all the NSSO
models. Fig.14 summarizes the total energies calculated for the
different relaxed configurations. Model, in which Eu occupies
Sr(II) site and nitrogen occupies O5' site, has the lowest energy,
indicating that this is the most stable configuration for NSSO and
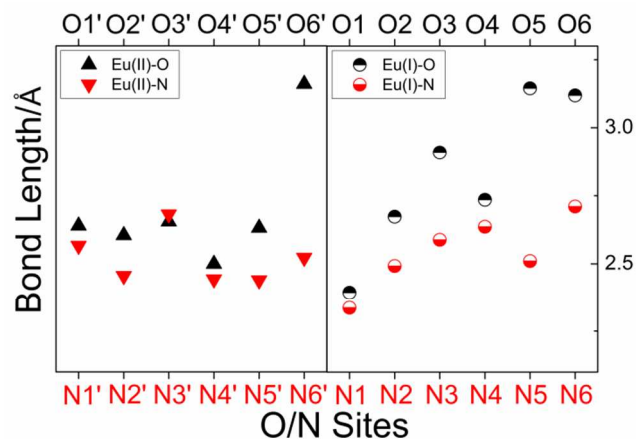25 will be used for further calculations.

Fig. 15 The bond length variation before and after nitrogen replacing the
specific oxygen atom.

The bond length distributions of Eu-O in two SSO models and
30 Eu-N in twelve NSSO models are shown in Fig.15. The bond
lengths almost all become shortened after the oxygen being
replaced by nitrogen. For example, obvious shortening appears in
Eu2N5' model, which is the most stable configuration for NSSO.
Based on these results, we can ascribe the shorter coordination
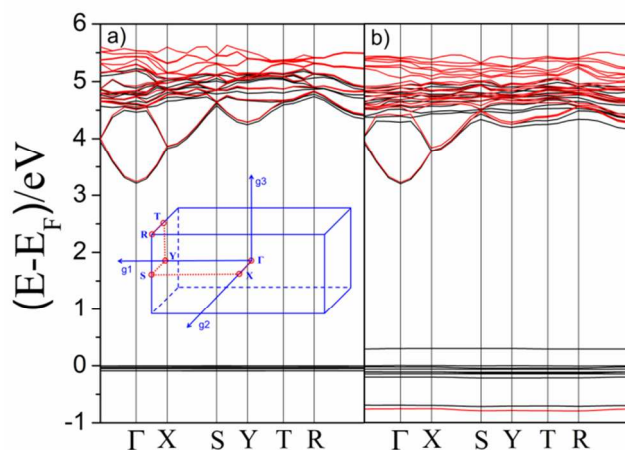35 distance shown in Fig.11 to the shortened Eu-N bonds after
nitrogen incorporation.

Fig. 16 Band structure of SSO (Eu2, a) and NSSO (Eu2N5', b) models, the inset indicates the Brillouin zone path for band structure calculation.

In order to illustrate the red emission of NSSO, we calculate the band structures of SSO and NSSO, as shown in Fig.16. For clarity, the Fermi level is set to zero. It lies right at the top of the Eu*4f* manifold (i.e., valence bands). These bands are of low band energy dispersion in E(k), indicating large joint density of states, hence large optical absorption and luminescence.[41] Since the PL properties are mainly determined by the top of the valence band (VB) and the bottom of the conduction band (CB), the density of states (DOS) and atom-resolved partial DOS (PDOS) of SSO and NSSO are shown in Fig.17 to 18, respectively.
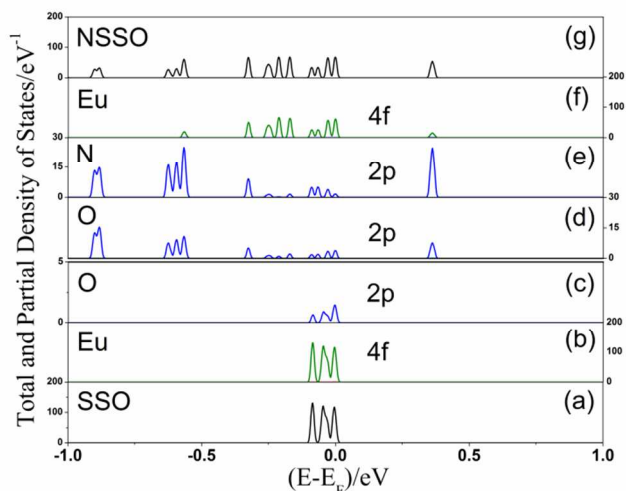

Fig. 17 DOS (a, g) and PDOS (b-f) near valence band of SSO (a-c) and NSSO (d-g) models, blue line represents p orbital and green line refers to f orbital.

As shown in the DOS and PDOS at the top of VB in Fig.17, sharp DOS peaks around Fermi level in SSO are mainly Eu 4f electrons and a minor portion of O 2p electrons. While for the NSSO model, the broad states include several components. The lowest states are composed of 2p electrons of nitrogen and oxygen atoms. The other states are hybrid orbitals of the Eu 4f electrons and 2p electrons of nitrogen and oxygen. So, the short nitrogen coordination distance of Eu leads to the hybridization of Eu 4f states and nitrogen/oxygen 2p states, which contributes to the broadened energy states.
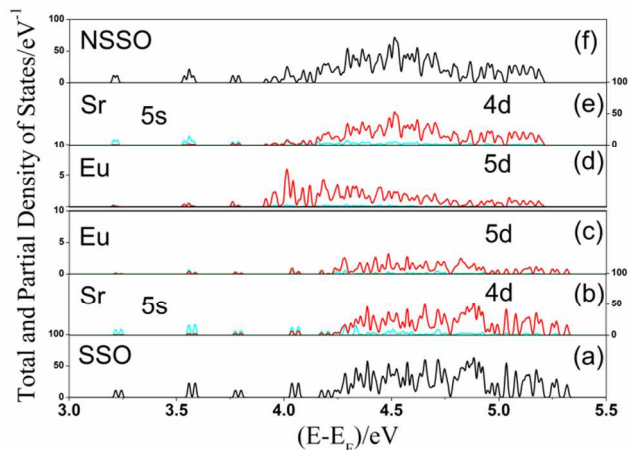

Fig. 18 DOS (a, f) and PDOS (b-e) near conduction band of SSO (a-c) and NSSO (d-f) models, red line indicates d orbital and cyan line indicates s orbital.

As could be seen in Fig.18, the lower part of the conduction bands is mostly contributed by Sr 5s, Sr 4d and Eu 5d states. Compared with SSO, the Eu 5d states in NSSO models shift to lower energy and their center of gravity also significantly moves to lower energy area. This, in combination with the broadened 4f like states of Eu, leads to the novel red-emission of the PL properties. This variation could also be attributed to the strengthened crystal field effects and nephelauxetic effects caused by the nitrogen coordination of Eu ions.

4 Conclusions

Extra red emission with high thermal stability could be achieved by the incorporation of a low amount of nitrogen into the $Sr_2SiO_4:Eu^{2+}$ phosphors, which could be attributed to the modification of the local coordination environment of the Eu ions. The modification has been confirmed by both experimental measurements and theoretical simulation. Nitrogen prefers to substitute O5' site around Eu in Sr(II) sites of Sr_2SiO_4, and the more covalent and shorter Eu-N bonds enable the broadening of Eu 4f energy states and the lower energy shifting of Eu 5d energy band, leading to the extra red-emission.
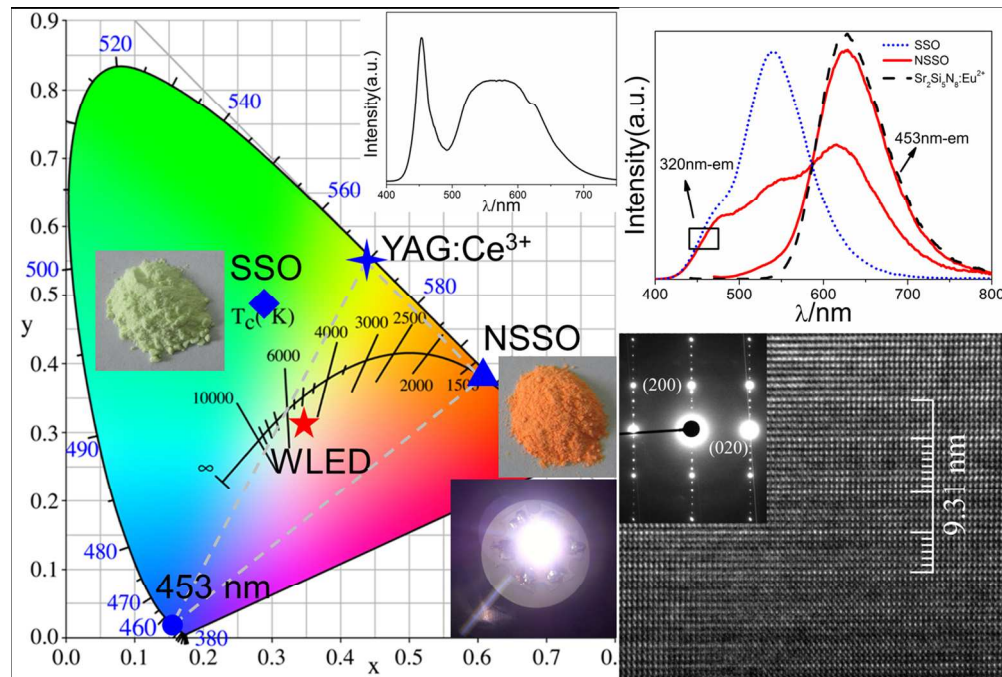
Acknowledgments

Notes and references

[a]CAS Key Laboratory of Materials for Energy Conversion, Department of Materials Science and Engineering, University of Science and

Technology of China, Hefei Anhui 230026, P.R. China. Fax: +86-551-63601592; Tel: +86-551-63600824; E-mail: xuxin@ustc.edu.cn
bHefei National Laboratory for Physical Sciences at the Microscale, University of Science and Technology of China, Hefei Anhui 230026, P.R. China
cDepartment of Physics, Tamkang University, New Taipei City 25137, Taiwan

1. C. He, Y. Guan, L. Yao, W. Cai, X. Li and Z. Yao, *Mater Res Bull*, 2003, **38**, 973.
2. C. Guo, D. Huang and Q. Su, *Materials Science and Engineering: B*, 2006, **130**, 189.
3. K. Uheda, N. Hirosaki, Y. Yamamoto, A. Naito, T. Nakajima and H. Yamamoto, *Electrochem Solid State Lett*, 2006, **9**, H22.
4. H. Watanabe and N. Kijima, *J Alloys Compd*, 2009, **475**, 434.
5. T. Suehiro, R.-J. Xie and N. Hirosaki, *Ind Eng Chem Res*, 2014, **53**, 2713.
6. S. E. Brinkley, N. Pfaff, K. A. Denault, Z. Zhang, H. T. Hintzen, R. Seshadri, S. Nakamura and S. P. DenBaars, *Appl Phys Lett*, 2011, **99**, 1106.
7. V. D. Luong, W. Zhang and H.-R. Lee, *J Alloys Compd*, 2011, **509**, 7525.
8. H. Nersisyan, H. l. Won and C. W. Won, *Chemical Communications*, 2011, **47**, 11897.
9. A. G. Kirakosyan and D. Y. Jeon, *J Electrochem Soc*, 2012, **159**, J29.
10. Y. Q. Li, J. E. J. van Steen, J. W. H. van Krevel, G. Botty, A. C. A. Delsing, F. J. DiSalvo, G. de With and H. T. Hintzen, *J Alloys Compd*, 2006, **417**, 273.
11. C. W. Yeh, W. T. Chen, R. S. Liu, S. F. Hu, H. S. Sheu, J. M. Chen and H. T. Hintzen, *J Am Chem Soc*, 2012, **134**, 14108.
12. T. Suehiro, R.-J. Xie and N. Hirosaki, *Ind Eng Chem Res*, 2013, **52**, 7453.
13. X. Q. Piao, T. Horikawa, H. Hanzawa and K. Machida, *Appl Phys Lett*, 2006, **88**, 1908.
14. T. Suehiro, N. Hirosaki and R. J. Xie, *ACS applied materials & interfaces*, 2011, **3**, 811.
15. J. K. Park, M. A. Lim, C. H. Kim, H. D. Park, J. T. Park and S. Y. Choi, *Appl Phys Lett*, 2003, **82**, 683.
16. X. Sun, J. Zhang, X. Zhang, S. Lu and X. Wang, *J Lumin*, 2007, **122**, 955.
17. I. Baginskiy, R. S. Liu, C. L. Wang, R. T. Lin and Y. J. Yao, *J Electrochem Soc*, 2011, **158**, P118.
18. B. G. Hyde, J. R. Sellar and L. Stenberg, *Acta Crystallographica Section B*, 1986, **42**, 423.
19. M. Catti, G. Gazzoni and G. Ivaldi, *Acta Crystallogr, Sect C: Cryst Struct Commun*, 1983, **39**, 29.
20. L.-C. Ju, C. Cai, Q.-Q. Zhu, J.-Y. Tang, L.-Y. Hao and X. Xu, *Journal of Materials Science: Materials in Electronics*, 2013, **24**, 4516.
21. A. Nag and T. R. N. Kutty, *J Mater Chem*, 2004, **14**, 1598.
22. K. C. Mishra, M. E. Hannah, A. Piquette, V. Eyert, P. C. Schmidt and K. H. Johnson, *ECS J Solid State Sci Technol*, 2012, **1**, R87.
23. H. He, R. Fu, X. Zhang, X. Song, X. Zhao and Z. Pan, *J Mater Sci - Mater Electron*, 2009, **20**, 433.
24. J. Park, S. J. Lee and Y. J. Kim, *Crystal Growth & Design*, 2013, **13**, 5204.
25. S. J. Lee, S.-H. Hong and Y. J. Kim, *J Electrochem Soc*, 2012, **159**, J163.
26. Z. Zhao, Z. Yang, Y. Shi, C. Wang, B. Liu, G. Zhu and Y. Wang, *Journal of Materials Chemistry C*, 2013, **1**, 1407.
27. G. Denis, X. Rocquefelte, P. Deniard, M. H. Whangbo and S. Jobic, *J Mater Chem*, 2009, **19**, 9170.
28. W. B. Im, Y.-l. Kim, H. S. Yoo and D. Y. Jeon, *Inorganic Chemistry*, 2009, **48**, 557.
29. Y.-F. Wang, Q.-Q. Zhu, L.-Y. Hao, X. Xu, R.-J. Xie, S. Agathopoulos and A. Srivastava, *J Am Ceram Soc*, 2013, **96**, 2562.
30. J.-Y. Tang, J.-K. Gao, J.-H. Chen, L.-Y. Hao, X. Xu and M.-H. Lee, *Computational Materials Science*, 2013, **79**, 478.
31. J. H. Lee and Y. J. Kim, *Mater Sci Eng B-Solid State Mater Adv Technol*, 2008, **146**, 99.
32. X. Piao, K. Machida, T. Horikawa and B. Yun, *J Lumin*, 2010, **130**, 8.
33. H. S. Jang, Y. H. Won and D. Y. Jeon, *Applied Physics B-Lasers and Optics*, 2009, **95**, 715.
34. J. K. Park, C. H. Kim, S. H. Park, H. D. Park and S. Y. Choi, *Appl Phys Lett*, 2004, **84**, 1647.
35. Y. P. Varshni, *Physica*, 1967, **34**, 149.
36. M. Catti, G. Gazzoni, G. Ivaldi and G. Zanini, *Acta Crystallogr, Sect B: Struct Sci*, 1983, **39**, 674.
37. R.-J. Xie, N. Hirosaki, T. Suehiro, F.-F. Xu and M. Mitomo, *Chemical Materials*, 2006, **18**, 5578.
38. H. Liu, Y. Hao, H. Wang, J. Zhao, P. Huang and B. Xu, *J Lumin*, 2011, **131**, 2422.
39. J. Weil and J. Bolton, *John Wiley & Sons, Ltd., New York*, 2007.
40. J. Tang, J. Chen, L. Hao, X. Xu, W. Xie and Q. Li, *J Lumin*, 2011, **131**, 1101.
41. J. G. Sole, L. E. Bausa and D. Jaque, *John Wiley & Sons, Ltd., New York*, 2005.

258x173mm (150 x 150 DPI)